Crystal structure of the calcium pump with a bound ATP analogue

Chikashi Toyoshima & Tatsuaki Mizutani*

Institute of Molecular and Cellular Biosciences, The University of Tokyo, Bunkyo-ku, Tokyo 113-0032, Japan

* Present address: Department of Immunology, Graduate School of Medicine, The University of Tokyo, Bunkyo-ku, Tokyo 113-0033, Japan

P-type ATPases are ATP-powered ion pumps that establish ion concentration gradients across cell and organelle membranes. Here, we describe the crystal structure of the Ca^{2+} pump of skeletal muscle sarcoplasmic reticulum, a representative member of the P-type ATPase superfamily, with an ATP analogue, a Mg^{2+} and two Ca^{2+} ions in the respective binding sites. In this state, the ATP analogue reorganizes the three cytoplasmic domains (A, N and P), which are widely separated without nucleotide, by directly bridging the N and P domains. The structure of the P-domain itself is altered by the binding of the ATP analogue and Mg^{2+}. As a result, the A-domain is tilted so that one of the transmembrane helices moves to lock the cytoplasmic gate of the transmembrane Ca^{2+}-binding sites. This appears to be the mechanism for occluding the bound Ca^{2+} ions, before releasing them into the lumen of the sarcoplasmic reticulum.

P-type ATPases are ion pumps that transfer cations across lipid bilayers. They establish ion concentration gradients that are used in a variety of biological processes and are referred to as such because they form a key phosphorylated intermediate in the reaction cycle (Fig. 1, inset; see ref. 1 for a review). The pumping of ions is thought to be achieved by altering the affinity and accessibility of the transmembrane ion-binding sites. Classical E1/E2 theory postulates that, in the E1 state, the binding sites have high affinity and open to the cytoplasm, whereas in the E2 state, the binding sites have low affinity and face the extracellular or lumenal side[2–4]. One important feature of the pumping process is that, before being released, bound cations are occluded; that is, become inaccessible from either side of the membrane. Binding in itself does not lock the cytoplasmic gate, and bound cations can be exchanged with those in the cytoplasm (reviewed in ref. 5). Occlusion is generally thought to require phosphoryl transfer from ATP to the ATPase. Release of cations into the extracellular or lumenal medium takes place while the enzyme is phosphorylated. Such autophosphorylation of the enzyme is a unique feature of P-type ATPases, and is distinct from other ATPases such as the F_0F_1 type.

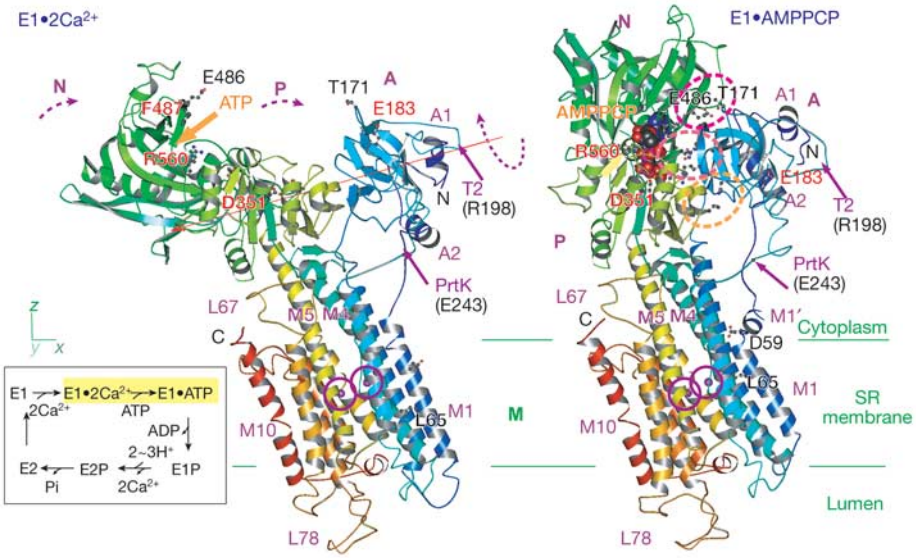

Figure 1 Front views (parallel to the membrane (*x*–*y*) plane) of Ca^{2+}-ATPase with (E1·AMPPCP) and without (E1·$2Ca^{2+}$) AMPPCP (shown in space fill), an ATP analogue, in the presence of 10 mM Ca^{2+}. Colours change gradually from the amino terminus (blue) to the carboxy terminus (red). Purple spheres (circled) represent bound Ca^{2+}. Large arrows in E1·$2Ca^{2+}$ indicate the direction of movements of the cytoplasmic domains (A, N and P) in the E1·$2Ca^{2+}$ → E1·AMPPCP transition; the axis of tilting of the A-domain is also specified (thin red line). α-Helices in the A-domain (A1 and A2) and those in the transmembrane domain (M1, M4, M5 and M10) are indicated. M1′ is an amphipathic part lying on the bilayer surface. PtrK, a proteinase-K digestion site (around Glu 243 (ref. 16)); SR, sarcoplasmic reticulum; T2, a trypsin digestion site at Arg 198 (ref. 10); ATP, the binding pocket for the adenosine moiety of ATP. Several key residues—E183 (A), F487 (N, adenine binding), D351 (P, phosphorylation site), R560 (N, β-phosphate binding) and those involved in interdomain hydrogen bonds (including T171 and E486)—are shown in ball-and-stick representation. Dotted circles indicate three contact spots between A- and N-domains (magenta) and between A- and P-domains (yellow). The figure was prepared with Molscript[44]. Inset is a simplified reaction scheme (showing only the forward direction); the two states compared here are shown with a yellow background.

Of the P-type ATPase superfamily, the Ca^{2+}-ATPase (SERCA1a) of fast skeletal muscle sarcoplasmic reticulum is structurally[6–8] and functionally[9] the best-characterized member. It is an integral membrane protein with a relative molecular mass of 110,000 (M_r, 110K)[10,11], consisting of three (A (actuator), N (nucleotide binding) and P (phosphorylation)) cytoplasmic domains and ten (M1–M10) transmembrane helices[6]. Two high-affinity Ca^{2+}-binding sites are located side-by-side within the transmembrane region, formed by M4, M5, M6 and M8 helices[6]. We have already published crystal structures of the Ca^{2+}-ATPase in a Ca^{2+}-bound state[6] ($E1{\cdot}2Ca^{2+}$; Protein Data Bank (PDB) accession code 1SU4) and a Ca^{2+}-unbound state[7] (E2(TG); PDB accession code 1IWO) stabilized by a potent inhibitor, thapsigargin (TG)[12]. A brief overview of these structures is found in ref. 13.

Here we report the crystal structure of SERCA1a with a non-hydrolysable ATP analogue—adenosine 5′-[β,γ-methylene]triphosphate (AMPPCP)—and a Mg^{2+} bound to the cytoplasmic domains, and two Ca^{2+} ions at the transmembrane binding sites. This structure (which we abbreviate to E1·AMPPCP) probably represents the one just before phosphoryl transfer from ATP to the enzyme, and explains how the γ-phosphate and Mg^{2+} binding to the P-domain results in the occlusion of the bound Ca^{2+} some 50 Å away.

Structure determination

Two types of crystals belonging to different space groups ($P2_1$ and $C2$) were grown by dialysing affinity-purified enzyme against a buffer containing 0.5 mM AMPPCP in the presence of 10 mM Ca^{2+} and 5 mM Mg^{2+}. Diffraction data were highly anisotropic and showed good statistics to 2.9 Å resolution after merging. The structure was determined by generalized molecular replacement[14], because heavy atom isomorphous replacement was unsuccessful. The atomic model was refined with the $P2_1$ crystals to an R_{free} value of 29.6%.

Rearrangement of the cytoplasmic domains

The binding of AMPPCP and a metal ion to Ca^{2+}-ATPase in $E1{\cdot}2Ca^{2+}$ causes large and global changes in the structure (Figs 1 and 2; see also Supplementary Movie), except for the transmembrane helices M6–M10. The most prominent difference is that the three cytoplasmic domains, widely separated in $E1{\cdot}2Ca^{2+}$, now form a compact headpiece. Gathering of the cytoplasmic domains also occurs in the E2(TG) state[7] but the arrangements are different (Supplementary Fig. 1). Notably, the N-domain is more inclined towards the P-domain. This inclination is facilitated by AMPPCP, whose adenine ring binds to the N-domain around Phe 487 whereas the γ-phosphate binds to the P-domain around Asp 351, the residue of phosphorylation. As a result of the large inclination, the N-domain now makes contacts with the A-domain (Fig. 1) with an interface that is different compared with E2(TG). Despite the ~90° inclination, only small changes are observed within the N-domain itself (root mean square deviation (r.m.s.d.) = 0.74 Å) except for a flexible loop (Pro 500–Gly 509) at the top of the molecule. In contrast, the P-domain changes its structure (see below) and also its orientation with respect to the membrane plane (~15°; Fig. 1). As a result of these changes, the A-domain is tilted by ~30° around an axis approximately parallel to the membrane (specified in Fig. 1), bringing the M2 side of the A-domain higher up (Fig. 2a).

Locking of the cytoplasmic gate

The position of the A-domain in E1·AMPPCP is in marked contrast with that in E2(TG) (Supplementary Fig. 1), where the A-domain is rotated ~110° from the position in $E1{\cdot}2Ca^{2+}$ around an axis

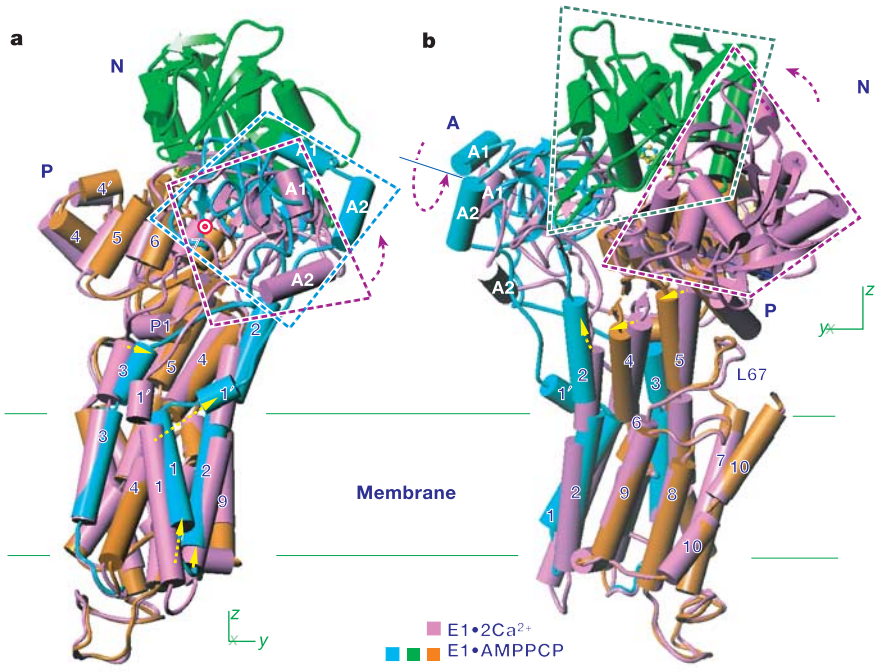

Figure 2 Superimposition of the $E1{\cdot}2Ca^{2+}$ and E1·AMPPCP forms of Ca^{2+}-ATPase fitted with the transmembrane domain. $E1{\cdot}2Ca^{2+}$, violet; E1·AMPPCP, cyan (A-domain and M1–M3 helices), light green (N-domain) and orange (P-domain and M4–M10 helices). α-Helices are represented by cylinders and β-strands by arrows. Both (**a** and **b**) are viewed along the membrane plane, but at a difference of 45°. M2, M3 and M5 are represented by two or three cylinders, although they are continuous helices. Helices in the A-domain (A1 and A2), P-domain (4–7) and transmembrane helices are indicated. The position of a preserved hydrogen bond between the A- and P-domains (Gly 156–Ala 725) is indicated by a double circle for $E1{\cdot}2Ca^{2+}$. Large arrows indicate the direction of movements of the cytoplasmic domains (A, N and P) in the $E1{\cdot}2Ca^{2+} \rightarrow$ E1·AMPPCP transition, and small ones those of transmembrane helices. Broken lines enclose the A-domain (**a**) and the N-domain (**b**). A thin blue line in **b** specifies the axis of tilting of the A-domain.

perpendicular to the membrane[7]. Because the A-domain is directly linked to the M1–M3 transmembrane helices, its movement inevitably causes rearrangements of these helices.

Of the three helices, M3 shows the smallest movement on nucleotide binding: only the top part is bent towards M2 by ~20° (Fig. 2a), although the loop connecting to the A-domain moves almost 20 Å (at Met 239) and appears to be strained, as indicated by the protection against proteinase K attack at Glu 243 (refs 15–17). The M2 helix shows a large and complex movement. M2 moves towards the cytoplasm by one turn of α-helix, presumably pulled by the tilt of the A-domain (Fig. 2a), and its cytoplasmic end shifts in a $+y$-direction (Fig. 2b). The M1 helix shows a marked movement: it is pulled towards the cytoplasmic side by nearly two turns of α-helix ($\Delta z = 8.3$ Å for Leu 65; Fig. 1), and is bent largely at Asp 59, so that the amphipathic amino-terminal part (M1′) lies on the membrane surface (Fig. 2a). This situation is very similar to that in E2(TG)[7], and the part lying on the membrane surface (Trp 50–Glu 58) is identical. However, there is an ~90° difference in the direction of bending so that M1′ approaches the M2 helix (that is, $+y$- instead of $+x$-direction as in E2(TG); Fig. 2a), reflecting the difference in orientation of the A-domain.

The functional meaning of the movement of the M1 helix is evident in the present structure. In E1·2Ca^{2+}, which represents the state after the binding of both Ca^{2+} ions, Glu 309 caps the Ca^{2+} in site II (Fig. 3a, c)[6]. On its cytoplasmic side, there is a large empty space in which several water molecules were identified in the crystal structure (Fig. 3a)[6]. Thus, it seems possible for Glu 309 to adopt other side-chain conformations. In E1·AMPPCP, however, this space is occupied by M1 (Fig. 3b), and Leu 65 on the M1 helix makes van der Waals contacts with the Glu 309 side chain (Fig. 3b, c). Glu 309 now forms a hydrogen bond with Asn 796 instead of with Glu 58 as in E1·2Ca^{2+} (Fig. 3). Thus, the conformation of Glu 309 is doubly locked.

It is well established that Ca^{2+} in site II is the second Ca^{2+} to bind[18,19] and is exchangeable with Ca^{2+} in the cytoplasm[5,20]. There is now strong evidence to indicate that Glu 309 works as the gating residue[21,22]. It is easy to see that site II Ca^{2+} will be ready to dissociate, if the Glu 309 carboxyl detaches from it by thermal movement. Virtually no Ca^{2+} exchange takes place in E1·AlF_x·ADP, indicating that the Ca^{2+} ions are occluded. Moreover, the Glu309Gln mutant cannot occlude at all whereas the Asn796Ala mutant can to a certain extent[22]. On the other hand, biochemical data[20] show that binding of AMPPCP itself is not sufficient to occlude bound Ca^{2+}, despite the fact that the crystal structures of E1·AMPPCP and E1·AlF_x·ADP (C.T., H. Nomura and T. Tsuda, unpublished data) are virtually the same except for details around the phosphorylation site. They also show very similar resistance to proteinase K attack at Glu 243 (Fig. 1)[15,16]. Extra stability provided by AlF_x, a stable analogue of phosphate, may account for the difference in dissociation kinetics. Also, crystal packing may have selected a specific conformation from many possible ones in solution. Nonetheless, taken together, it seems clear that the locking of the conformation of Glu 309 by M1 helix is the mechanism of occlusion. A key residue here is Leu 65, as also demonstrated by a mutagenesis study[23].

In the E2(TG) form, the P-domain is inclined ~30° compared with the E1·2Ca^{2+} form[7]. This inclination brings about a large downward movement (~5.5 Å) of the M4 helix and destroys the Ca^{2+}-binding sites. In E1·AMPPCP, the P-domain is inclined in the same direction but only by about half as much as in E2(TG), because

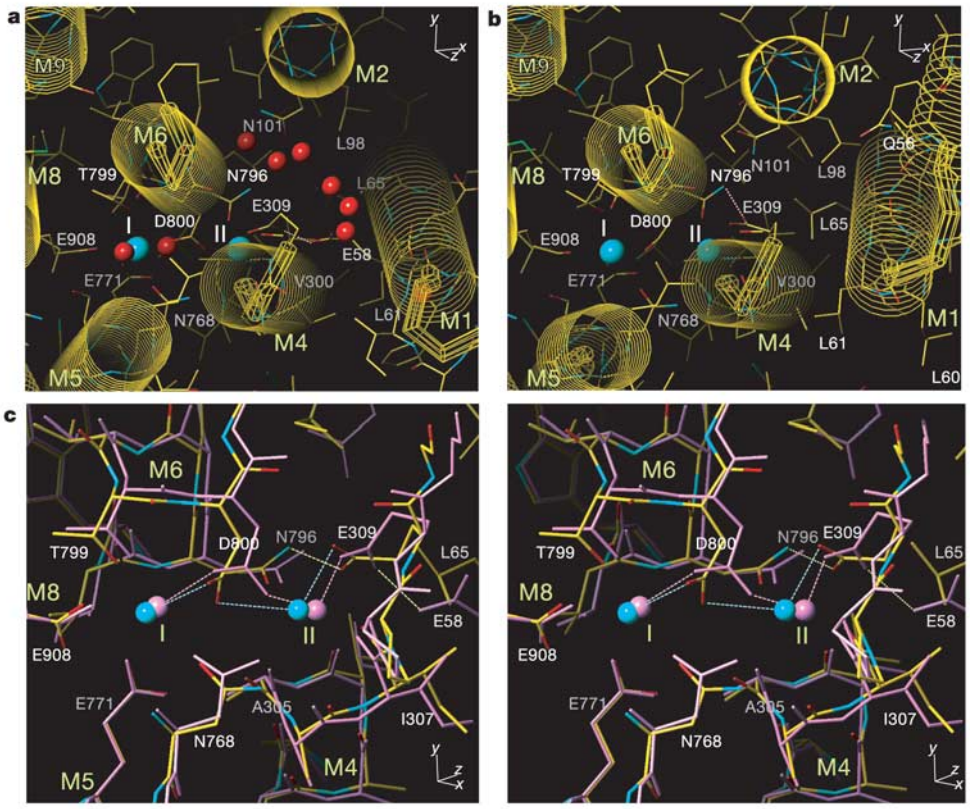

Figure 3 Transmembrane Ca^{2+}-binding sites (I and II) and the movement of the M1 helix. **a**, E1·2Ca^{2+}; **b**, E1·AMPPCP; **c**, superimposition of E1·2Ca^{2+} (violet) and E1·AMPPCP (atom colour) in stereo view. Cyan (**a**–**c**) and violet spheres (**c**) represent bound Ca^{2+}; red spheres indicate water molecules in the crystals. Owing to the resolution limitation of the diffraction data, no water molecules are shown in **b**. Dotted lines in **c** show the coordination of Ca^{2+} and hydrogen bonds involving E309 and D800 side chains.

bound Ca^{2+} restricts the bending of M5. The upper part of M4 certainly shows a downward movement (Fig. 2b)[7]. It is compensated, however, by the bending of the P-domain (see below) and is 'absorbed' by the unwound part containing Glu 309. To achieve this, Glu 309 appears to alter its main-chain conformation, but also pushes site II Ca^{2+} and Asp 800 (Fig. 3c). As a result, the coordination geometry of the Ca^{2+} becomes loose, particularly at site II. This change presumably prepares for the release of bound Ca^{2+} to the lumen during the conversion to E2P, the subsequent step in the reaction cycle.

ATP as a cleavable crosslinker

As described in the preceding sections, the large inclination of the N-domain is important for orientating the A-domain to close the cytoplasmic gate. AMPPCP facilitates this by crosslinking the N- and P-domains (Fig. 4). The conformation of AMPPCP appears to be rather uncommon: the phosphate moiety adopts a zigzag configuration, similar to that in the histidine kinase CheA (PDB accession code 1I58)[24], bringing the β-phosphate close to the ribose. The orientation of the ribose and the configuration of the phosphates are different compared with those observed with the NMR structure of ATP bound to the isolated N-domain of Na^+K^+-ATPase with no Mg^{2+} (ref. 25). The adenine ring of AMPPCP is positioned predominantly by stacking with Phe 487, consistent with previous results[6,25,26] (Fig. 4a). Hydrogen bonding with main-chain carbonyl and amide groups, found with many adenosine-binding proteins[27], is not observed here. Instead, a ribose hydroxyl (O3*) is stabilized by Arg 678, which in turn appears to form hydrogen bonds with residues both in the N- and P-domains (Fig. 4b). The O2* of the ribose may also contribute to the positioning of the ribose by van der Waals contacts. These features are consistent with infrared spectroscopy studies[28]. The α-phosphate is stabilized by Arg 489 (Fig. 4a) and the β-phosphate by Arg 560, which also appears to form hydrogen bonds with residues both in the N- and P-domains (Fig. 4b). Within a 3.4 Å distance from the γ-phosphate, there is a carboxyl group of Asp 351, hydroxyl groups of Thr 353 and Thr 625, amide groups of Thr 353 and Gly 626, a carbonyl group of Thr 353 and a metal ion (modelled as Mg^{2+}; see Supplementary Methods) plus two coordinating water molecules. Asn 706 and Lys 684 are slightly more distant. Although the accuracy of such information is limited at 2.9 Å resolution, all of these residues have been identified as being sensitive to mutation[29–31]. No bridging Mg^{2+} is found between the β- and γ-phosphates, presumably because Asp 627 blocks proper octahedral coordination of Mg^{2+}.

An intricate network of hydrogen bonds thus appears to be formed around AMPPCP (Fig. 4b), including those bridging the N- and P-domains. Of the residues involved in such bridging interactions, mutagenesis studies have shown that Arg 560 on the N-domain is particularly important[17,32,33]. This residue appears to orientate the phosphate chain of AMPPCP in the right direction and form a salt bridge with Asp 627 in the P-domain, thereby establishing the N-domain–P-domain interaction. The importance of Arg 560 indicates that an oxygen atom of the β-phosphate has a key role in positioning this residue mobile in E1·2Ca^{2+} and also suggests that the N-domain will move back when ADP leaves the enzyme. It is well known that acetylphosphate and carbamoylphosphate are substrates of Ca^{2+}-ATPase[34], and indeed both of them have an oxygen atom at this position.

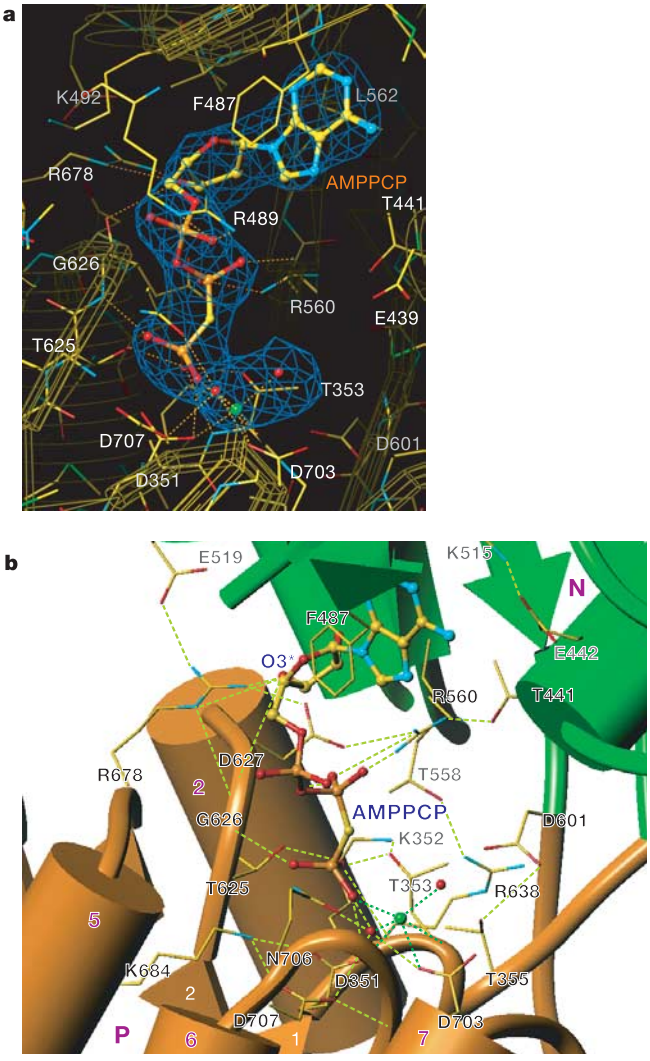

Figure 4 Omit-annealed $F_o - F_c$ map around AMPPCP at 5σ (**a**) and the hydrogen-bonding network around AMPPCP (**b**). AMPPCP is shown in ball-and-stick representation; the N- and P-domains are coloured light green and orange, respectively. Light-green broken lines in **b** show likely hydrogen bonds. A part of the N-domain is removed for clarity. Small spheres represent Mg^{2+} (green) and two water molecules (red), which coordinate to the Mg^{2+}, together with γ-phosphate, carboxyl groups of Asp 351 and Asp703, and a carbonyl group of Thr 353 (orange broken lines in **a** and dark-green lines in **b**).

Changes in the P-domain structure

On binding the γ-phosphate and Mg^{2+}, the P-domain changes its internal structure and its overall orientation with respect to the M5 helix (Fig. 5). As a member of the haloacid dehalogenase superfamily[35], the P-domain of Ca^{2+}-ATPase comprises a Rossmann fold that consists of a central seven-stranded (Pβ1–Pβ7) parallel β-sheet and associated helices (Pα1–Pα7)[6]. A unique feature of the β-sheet in Ca^{2+}-ATPase is that the two halves (Pβ1–Pβ4 and Pβ5–Pβ7) are staggered in unphosphorylated forms, but have a better alignment in phosphorylated (or γ-phosphate bound) forms (Fig. 5a). The top part of the first half (Pβ1–Pβ4) moves together as a result of binding of the γ-phosphate and Mg^{2+}, because Thr 353 positioned just above Pβ1 coordinates to both ligands (Figs 4b and 5). Thr 625 and Gly 626 in the loop connecting Pβ2 and Pα2 appear to coordinate to the γ-phosphate (Fig. 4). Furthermore, Pβ5 twists upon binding of Mg^{2+} owing to the coordination by Asp 703 (Figs 4 and 5), which causes the tilting of Pα5–Pα7. Thus, the P-domain is bent in nearly two orthogonal directions (Fig. 5).

This change in the β-sheet structure brings the N-domain ~30° closer to the P-domain and is presumably essential for achieving a nearly 90° inclination required for ATP to reach the P-domain. Thus, the staggered β-sheet works as a secondary hinge, in addition to the main one (around Pro 602 and Pro 603) that covers ~60° as in the E1·2Ca^{2+} → E2(TG) transition. This secondary hinge also changes the direction of movement of the N-domain (Fig. 5),

thereby forming a different interface with the A-domain.

The match of the P-domain with the catalytic domain in other members of the haloacid dehalogenase superfamily[35], such as phosphoserine phosphatase[36] and phosphoglucomutase[37], is rather poor in E1·2Ca^{2+} or E2(TG) form, but is much better in E1·AMPPCP (r.m.s.d. = 0.60 Å for 57 Cα atoms with phosphoserine phosphatase); the positions of Mg^{2+}, coordinating residues and two water molecules are also nearly identical. These features are understandable, because Ca^{2+}-ATPase requires much larger movements of the N-domain than the other members, such as phosphoserine phosphatase[36], while presumably using the same mechanism for phosphorylation and hydrolysis.

Positioning of the A-domain

The bending of the P-domain may also have a direct role in changing the orientation of the A-domain, which is tilted by ~30° around an axis approximately parallel to the membrane (Figs 1 and 2). This can be regarded as a rigid-body movement around a hydrogen bond between main chains of two conserved residues, Gly 156 (A-domain) and Ala 725 (P-domain). This hydrogen bond is present in both E1·2Ca^{2+} and E1·AMPPCP (Fig. 5), but it is unlikely to be enough for linking the A- and P-domains together. In E1·2Ca^{2+}, the A-domain appears to make a point contact with the P-domain (Fig. 5) and seems to be highly mobile: Gly 156–Lys 158, in a short loop sticking out from the A-domain, and Ala 725–Val 726 at the top of the P7 helix (Fig. 5b), are the only residues that come within a 4 Å distance.

This situation is not much different in E1·AMPPCP. Again, the interaction is limited to that around the P7 helix (Supplementary Fig. 2) but is more stable: the 'socket' on the P-domain is larger and one extra hydrogen bond appears to be formed (Supplementary Fig. 2). These apparently small differences in contacting residues, however, may be critical for changing the orientation of the A-domain, because the socket, the P7 helix, moves upwards and tilts so that the M2 side becomes higher up in the E1·2Ca^{2+} → E1·AMPPCP transition (Fig. 5b). Although small, this movement caused by the binding of the γ-phosphate and Mg^{2+} will be effective, because it occurs at the pivoting point.

The interface between the N- and A-domains is not complementary either (Fig. 6). There are only two contact spots located on either side of the apparent pivoting point (Fig. 1, dotted circles in red). Presumably the most important one is a kind of mechanical couple formed on the M3 side around a hydrogen bond between Thr 171 (A-domain) and Glu 486 (N-domain) (Fig. 6). On the M2 side, we can identify two salt bridges and three hydrogen bonds likely to be formed between the A- and N-domains. If the A-domain keeps to the same position as in E1·2Ca^{2+}, when the N-domain inclines Thr 484 (N-domain) would collide with Thr 171 and push the M3 side of the A-domain. This might be another cause of the A-domain tilting; however, its contribution is difficult to evaluate, because the P-domain inclines and moves the A-domain at the same time.

Considering that the A-domain has to rotate horizontally by more than 90° during the E1P → E2P transition, it is understandable that the A–N interface is not complementary (Fig. 5). The structure around Thr 171 is interesting in this regard, because it may provide a solid pivot for such rotations, and because Thr 171

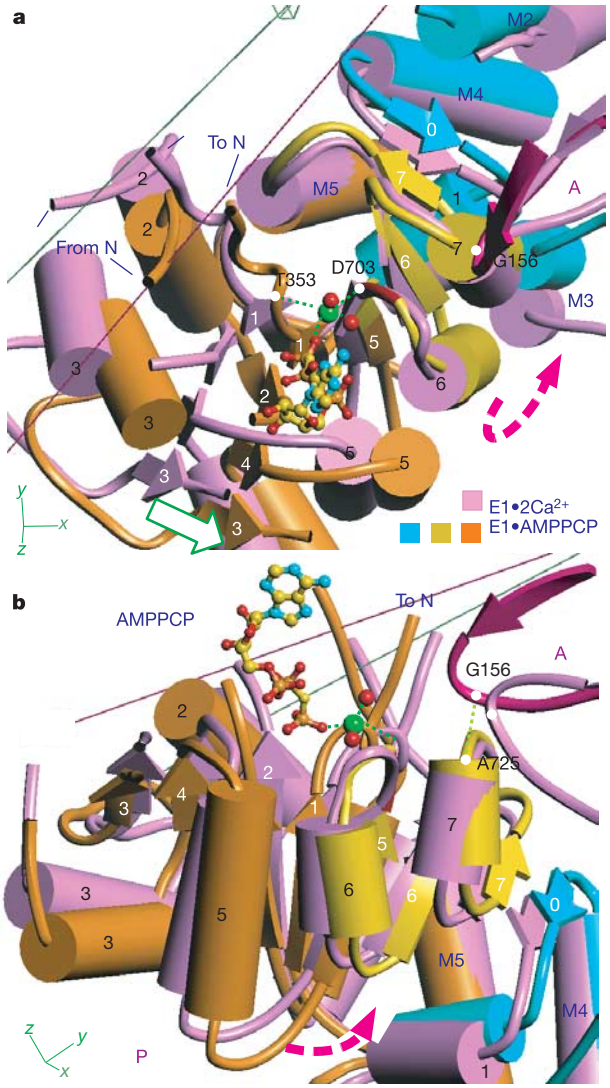

Figure 5 Superposition of the P-domain in E1·2Ca^{2+} and E1·AMPPCP, fitted with the 15 residues at the N-terminal end of the M5 helix. **a**, **b**, Top (**a**) and side (**b**) views. Colours representing E1·2Ca^{2+} and different regions of the P-domain in E1·AMPPCP, as recognized by Dyndom[45], are indicated. A part of the P-domain (containing helices 4 and 4′) is removed. Small spheres represent Mg^{2+} (green) and two water molecules (red). Two long lines specify the positions of the axis of the N-domain inclination for E2(TG) (green) and E1·AMPPCP (purple) as determined by Dyndom[45]. The green arrow in **a** indicates the movement of β-strands 1–4 in the E1·2Ca^{2+} → E1·AMPPCP transition, whereas those in red show the tilting of the α-helices 5–7.

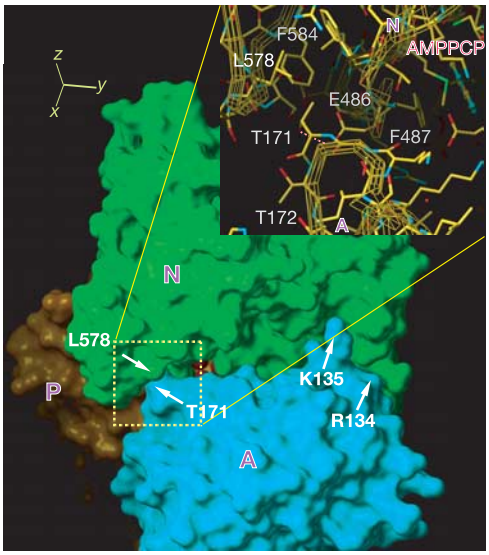

Figure 6 Water-accessible surface of the cytoplasmic domains in E1·AMPPCP showing the A–N interface. Inset is an enlarged view of the boxed area, where the A- and N-domains appear to be mechanically coupled.

interacts with Glu 486, the residue next to Phe 487, which is the primary residue for adenine binding. Hence, the binding and the release of ATP might directly affect the A–N interface. In fact the strand Nβ7, on which Glu 486 and Phe 487 are located (Fig. 6 inset), shows the largest movement in the N-domain upon binding of AMPPCP.

Discussion

From the crystal structures it is clear that Ca^{2+}-ATPase changes the orientation of the A-domain to regulate the cytoplasmic gate of the Ca^{2+}-binding pathway by moving, primarily, the M1 helix. This means that the interfaces between the A-domain and the two other cytoplasmic domains are critically important and adjusted during the reaction cycle. Here, ATP works as the principal modifier. It brings the N-domain very close to the P-domain by directly bridging them, so that the N domain can 'grip' the M3 side of the A-domain. To achieve this, the γ-phosphate bends the P-domain to gain an extra ~30° of inclination. At the same time, ATP induces the binding of Mg^{2+}, which bends the P-domain in a nearly orthogonal direction so that the M2 side is brought higher up. As a combined result of these interactions, the A-domain tilts by ~30° to pull up the M1–M2 helices and to strain the loop connecting to M3. This strain might be the driving force for another A-domain rotation that occurs in subsequent steps in the reaction cycle to open the lumenal gate. The extensive hydrogen-bonding network formed around the ATP (analogue) might be required for sustaining this strained state. □

Methods

Crystallization

Ca^{2+}-ATPase was prepared from rabbit hind-leg white muscle[38] and purified by affinity chromatography[39]; for elution AMPPCP was used. Crystals of $P2_1$ symmetry were prepared by dialysing purified enzyme (20 μM) mixed with phosphatidylcholine in detergent octaehyleneglycol mono-*n*-dedecylether ($C_{12}E_8$, 2 mg ml^{-1}) against a buffer consisting of 20% glycerol, 12% PEG 400, 10 mM $CaCl_2$, 5 mM $MgCl_2$, 2.5 mM NaN_3, 2 μg ml^{-1} butylhydroxytoluene, 0.2 mM dithiothreitol, 20 mM MES, pH 6.1, and 0.5 mM AMPPCP for about one month. Crystals were grown to 100 × 100 × 60 μm and flash-frozen in cold nitrogen gas in a cold room. For making *C*2 crystals, 200 mM sodium propionate was included in the dialysis buffer.

Data collection

All the diffraction data were collected at BL41XU, SPring-8, using a MAR165 CCD detector at λ = 0.72 Å, and processed with Denzo and Scalepack[40]. For refinement, diffraction data from two best crystals with $P2_1$ symmetry were merged (R_{merge} = 5.6% with a redundancy of 6.7 and I/σ = 27.0) for 1/15.0 to 1/2.9 Å^{-1} (24.0%, 3.10 and 3.58, respectively, for the highest-resolution bin, 3.00–2.9 Å). Unit cell dimensions were a = 90.9, b = 123.6, c = 151.8 Å and β = 107.2°. Two protein molecules were contained in the asymmetric unit.

Modelling and refinement

The crystal structure was determined by molecular replacement[14], first using the data from *C*2 crystals that contain only one protein molecule in an asymmetric unit. The starting model included the M4–M10 helices and the P-domain only. The N-domain was readily placed in the first map calculated from them, after solvent flattening with CNS[41]. The M3 helix and then the A-domain were added in the subsequent maps with no difficulty. Finally M1–M2 helices were constructed. The resulting atomic model was used as the starting model for refinement with the diffraction data from $P2_1$ crystals. The diffraction data contained 70,272 reflections at 99.4% completeness (from 15 to 2.9 Å resolution). The atomic model consisting of 7,709 × 2 atoms (7,671 in the protein, 31 in AMPPCP, 3 ions and 4 water) was refined at a 2.9 Å resolution to R_{cryst} of 25.2% and R_{free} of 29.6% using CNS[41] with a strong non-crystallographic symmetry restraint. r.m.s.d of the bond length and angle were 0.009 Å and 1.3°, respectively. The geometry of the model was examined with Procheck[42]; 992 out of 994 residues were in the most favourable or favourable region in the Ramachandran plot. The secondary structure was assigned with DSSP[43]. (More details are given in Supplementary Methods.)

Received 23 March; accepted 19 May 2004; doi:10.1038/nature02680.
Published online 30 June 2004.

1. Møller, J. V., Juul, B. & le Maire, M. Structural organization, ion transport, and energy transduction of P-type ATPases. *Biochim. Biophys. Acta* **1286,** 1–51 (1996).
2. Post, R. L., Hegyvary, C. & Kume, S. Activation by adenosine triphosphate in the phosphorylation kinetics of sodium and potassium ion transport adenosine triphosphatase. *J. Biol. Chem.* **247,** 6530–6540 (1972).
3. Albers, R. W. Biochemical aspects of active transport. *Annu. Rev. Biochem.* **36,** 727–756 (1967).
4. de Meis, L. & Vianna, A. L. Energy interconversion by the Ca^{2+}-dependent ATPase of the sarcoplasmic reticulum. *Annu. Rev. Biochem.* **48,** 275–292 (1979).
5. Mintz, E. & Guillain, F. Ca^{2+} transport by the sarcoplasmic reticulum ATPase. *Biochim. Biophys. Acta* **1318,** 52–70 (1997).
6. Toyoshima, C., Nakasako, M., Nomura, H. & Ogawa, H. Crystal structure of the calcium pump of sarcoplasmic reticulum at 2.6 Å resolution. *Nature* **405,** 647–655 (2000).
7. Toyoshima, C. & Nomura, H. Structural changes in the calcium pump accompanying the dissociation of calcium. *Nature* **418,** 605–611 (2002).
8. Xu, C., Rice, W. J., He, W. & Stokes, D. L. A structural model for the catalytic cycle of Ca^{2+}-ATPase. *J. Mol. Biol.* **316,** 201–211 (2002).
9. MacLennan, D. H., Rice, W. J. & Green, N. M. The mechanism of Ca^{2+} transport by sarco(endo)plasmic reticulum Ca^{2+}-ATPases. *J. Biol. Chem.* **272,** 28815–28818 (1997).
10. MacLennan, D. H., Brandl, C. J., Korczak, B. & Green, N. M. Amino-acid sequence of a Ca^{2+} + Mg^{2+}-dependent ATPase from rabbit muscle sarcoplasmic reticulum, deduced from its complementary DNA sequence. *Nature* **316,** 696–700 (1985).
11. Brandl, C. J., deLeon, S., Martin, D. R. & MacLennan, D. H. Adult forms of the Ca^{2+} ATPase of sarcoplasmic reticulum. Expression in developing skeletal muscle. *J. Biol. Chem.* **262,** 3768–3774 (1987).
12. Sagara, Y. & Inesi, G. Inhibition of the sarcoplasmic reticulum Ca^{2+} transport ATPase by thapsigargin at subnanomolar concentrations. *J. Biol. Chem.* **266,** 13503–13506 (1991).
13. Toyoshima, C., Nomura, H. & Sugita, Y. Structural basis of ion pumping by Ca^{2+}-ATPase of sarcoplasmic reticulum. *FEBS Lett.* **555,** 106–110 (2003).
14. Brünger, A. T. Extension of molecular replacement: a new search strategy based on Patterson correlation refinement. *Acta Crystallogr. A* **46,** 46–57 (1990).
15. Danko, S., Yamasaki, K., Daiho, T., Suzuki, H. & Toyoshima, C. Organization of cytoplasmic domains of sarcoplasmic reticulum Ca^{2+}-ATPase in E_1P and E_1ATP states: a limited proteolysis study. *FEBS Lett.* **505,** 129–135 (2001).
16. Juul, B. *et al.* Do transmembrane segments in proteolyzed sarcoplasmic reticulum Ca^{2+}-ATPase retain their functional Ca^{2+} binding properties after removal of cytoplasmic fragments by proteinase K? *J. Biol. Chem.* **270,** 20123–20134 (1995).
17. Ma, H., Inesi, G. & Toyoshima, C. Substrate-induced conformational fit and headpiece closure in the Ca^{2+}ATPase (SERCA). *J. Biol. Chem.* **278,** 28938–28943 (2003).
18. Andersen, J. P. & Vilsen, B. Amino acids Asn796 and Thr799 of the Ca^{2+}-ATPase of sarcoplasmic reticulum bind Ca^{2+} at different sites. *J. Biol. Chem.* **269,** 15931–15936 (1994).
19. Zhang, Z. *et al.* Detailed characterization of the cooperative mechanism of Ca^{2+} binding and catalytic activation in the Ca^{2+} transport (SERCA) ATPase. *Biochemistry* **39,** 8758–8767 (2000).
20. Orlowski, S. & Champeil, P. Kinetics of calcium dissociation from its high-affinity transport sites on sarcoplasmic reticulum ATPase. *Biochemistry* **30,** 352–361 (1991).
21. Vilsen, B. & Andersen, J. P. Mutation to the glutamate in the fourth membrane segment of Na^+, K^+-ATPase and Ca^{2+}-ATPase affects cation binding from both sides of the membrane and destabilizes the occluded enzyme forms. *Biochemistry* **37,** 10961–10971 (1998).
22. Inesi, G., Ma, H., Lewis, D. & Xu, C. Ca^{2+} occlusion and gating function of Glu309 in the fluoroaluminate analog of the Ca^{2+}-ATPase phosphoenzyme intermediate. *J. Biol. Chem.* (in the press).
23. Einholm, A. P., Vilsen, B. & Andersen, J. P. Importance of transmembrane segment M1 of the sarcoplasmic reticulum Ca^{2+}-ATPase in Ca^{2+} occlusion and phosphoenzyme processing. *J. Biol. Chem.* **279,** 15888–15896 (2004).
24. Bilwes, A. M., Quezada, C. M., Croal, L. R., Crane, B. R. & Simon, M. I. Nucleotide binding by the histidine kinase CheA. *Nature Struct. Biol.* **8,** 353–360 (2001).
25. Hilge, M. *et al.* ATP-induced conformational changes of the nucleotide-binding domain of Na,K-ATPase. *Nature Struct. Biol.* **10,** 468–474 (2003).
26. McIntosh, D. B., Woolley, D. G., Vilsen, B. & Andersen, J. P. Mutagenesis of segment ^{487}Phe-Ser-Arg-Asp-Arg-Lys^{492} of sarcoplasmic reticulum Ca^{2+}-ATPase produces pumps defective in ATP binding. *J. Biol. Chem.* **271,** 25778–25789 (1996).
27. Cappello, V., Tramontano, A. & Koch, U. Classification of proteins based on the properties of the ligand-binding site: the case of adenine-binding proteins. *Proteins* **47,** 106–115 (2002).
28. Liu, M. & Barth, A. Mapping interactions between the Ca^{2+}-ATPase and its substrate ATP with infrared spectroscopy. *J. Biol. Chem.* **278,** 10112–10118 (2003).
29. Clarke, D. M., Loo, T. W. & MacLennan, D. H. Functional consequences of alterations to amino acids located in the nucleotide binding domain of the Ca^{2+}-ATPase of sarcoplasmic reticulum. *J. Biol. Chem.* **265,** 22223–22227 (1990).
30. Maruyama, K. *et al.* Functional consequences of alterations to amino acids located in the catalytic center (isoleucine 348 to threonine 357) and nucleotide-binding domain of the Ca^{2+}-ATPase of sarcoplasmic reticulum. *J. Biol. Chem.* **264,** 13038–13042 (1989).
31. McIntosh, D. B., Woolley, D. G., MacLennan, D. H., Vilsen, B. & Andersen, J. P. Interaction of nucleotides with Asp^{351} and the conserved phosphorylation loop of sarcoplasmic reticulum Ca^{2+}-ATPase. *J. Biol. Chem.* **274,** 25227–25236 (1999).
32. Clausen, J. D., McIntosh, D. B., Vilsen, B., Woolley, D. G. & Andersen, J. P. Importance of conserved N-domain residues Thr441, Glu442, Lys515, Arg560, and Leu562 of sarcoplasmic reticulum Ca^{2+}-ATPase for MgATP binding and subsequent catalytic steps. Plasticity of the nucleotide-binding site. *J. Biol. Chem.* **278,** 20245–20258 (2003).
33. Jacobsen, M. D., Pedersen, P. A. & Jorgensen, P. L. Importance of Na,K-ATPase residue α1-Arg544 in the segment Arg544-Asp567 for high-affinity binding of ATP, ADP, or MgATP. *Biochemistry* **41,** 1451–1456 (2002).
34. McIntosh, D. B. The ATP binding sites of P-type ion transport ATPases. *Adv. Mol. Cell Biol.* **23A,** 33–99 (1998).
35. Aravind, L., Galperin, M. Y. & Koonin, E. V. The catalytic domain of the P-type ATPase has the haloacid dehalogenase fold. *Trends Biochem. Sci.* **23,** 127–129 (1998).
36. Wang, W. *et al.* Structural characterization of the reaction pathway in phosphoserine phosphatase: crystallographic 'snapshots' of intermediate states. *J. Mol. Biol.* **319,** 421–431 (2002).
37. Lahiri, S. D., Zhang, G., Dunaway-Mariano, D. & Allen, K. N. Caught in the act: the structure of phosphorylated β-phosphoglucomutase from *Lactococcus lactis*. *Biochemistry* **41,** 8351–8359 (2002).
38. Eletr, S. & Inesi, G. Phospholipid orientation in sarcoplasmic membranes: spin-label ESR and proton MNR studies. *Biochim. Biophys. Acta* **282,** 174–179 (1972).
39. Coll, R. J. & Murphy, A. J. Purification of the CaATPase of sarcoplasmic reticulum by affinity chromatography. *J. Biol. Chem.* **259,** 14249–14254 (1984).

40. Otwinowski, Z. & Minor, W. Processing of X-ray diffraction data collected in oscillation mode. *Methods Enzymol.* **276,** 307–325 (1997).
41. Brünger, A. T. *et al.* Crystallography & NMR system: A new software suite for macromolecular structure determination. *Acta Crystallogr. D* **54,** 905–921 (1998).
42. Collaborative Computational Project No. 4. The CCP4 suite: programs for protein crystallography. *Acta Crystallogr. D* **50,** 760–763 (1994).
43. Kabsch, W. & Sander, C. Dictionary of protein secondary structure: pattern recognition of hydrogen-bonded and geometrical features. *Biopolymers* **22,** 2577–2637 (1983).
44. Kraulis, P. J. MOLSCRIPT: a program to produce both detailed and schematic plots of protein structures. *J. Appl. Crystallogr.* **24,** 946–950 (1991).
45. Hayward, S. Structural principles governing domain motions in proteins. *Proteins* **36,** 425–435 (1999).

Supplementary Information accompanies the paper on **www.nature.com/nature**.

Acknowledgements We thank T. Tsuda for help in many aspects of this work; M. Kawamoto and H. Sakai for data collection at BL41XU of SPring-8; N. Miyashita for making many movies; and Y. Ohuchi for computer programs. We are grateful to D.B. McIntosh for help in improving the manuscript and G. Inesi for communicating unpublished results to us. This work was supported in part by a Creative Science Project Grant from the Ministry of Education, Culture, Sports, Science and Technology, the Japan New Energy and Industry Technology Development Organization, and the Human Frontier Science Program.

Competing interests statement The authors declare that they have no competing financial interests.

Correspondence and requests for materials should be addressed to C.T. (ct@iam.u-tokyo.ac.jp). The atomic coordinates are deposited in the PDB under accession code 1VFP.